Picturing the ionization process in ion-atom collisions with time-dependent quantum and classical methods

Clara Illescas[1], B. Pons[1] and A. Riera[2]

[1] *Centre Lasers Intenses et Applications, UMR 5107 du CNRS, Université de Bordeaux-I, 351 Cours de la Libération, F-33405 Talence, France*

[2] *Departamento de Química, C-IX, Universidad Autónoma de Madrid, Cantoblanco, E-28049 Madrid, Spain*

(December 2, 2002)

Abstract

The classical trajectory Monte Carlo method and the monocentric close-coupling Bessel expansion scheme are implemented to describe ionizing $He^{2+} + H(1s)$ collisions at the threshold of the high impact energy range. Ionization dynamics are pictured by showing the temporal evolution of both ionizing density and average velocity field. We emphasize that the classical and quantum mechanical treatments of electronic motion yield very close descriptions of ionization.

PACS numbers: 34.10.+x, 34.50.Fa

I. INTRODUCTION

Our intuitive interpretation of ionization dynamics in ion-atom collisions mostly rests on a classical, corpuscular interpretation of microscopic reality [1]. In addition, the success of the classical trajectory Monte Carlo (CTMC, [2,3]) method has strenghtened this interpetation, by predicting over a broad range of impact energies and collision systems, total and differential cross sections in close agreement with experiment (see e.g. [4-6]). In the classical approximation, all particles behave like macroscopic entities and obey Newtonian laws. Accordingly trajectories are associated to the motion of all particles, yielding collision scenarios that have more than once shed light on the main features of the ionization dynamics [7-9].

In principle, and because of the small electronic mass, the motion of the electrons should be described in terms of quantum mechanics. However, most of the time-dependent quantal treatments consist in expanding the total electronic wave function over finite sets of exponentially decaying basis functions, and such expansions cannot fairly reproduce the spread of the ionization cloud in the outgoing part of the collision, because of the inadequate short range character of the basis functions [10]. Alternative expansions and new integration schemes have been proposed during the last decade to better describe the ionizing cloud: the monocentric close-coupling expansions in terms of wavepackets and spherical Bessel functions by Schiwietz [11] and Pons [10] respectively, the Basis Generator Method (BGM) by Kroneisen *et al.* [12], direct numerical integration of the Time Dependent Schrodinger Equation (TDSE) by Wells *et al.* [13], the Two Center Momentum Space Discretization (TCMSD) method by Sidky and Lin [14]. The main contribution of these methods to our undertanding of the ionization dynamics consists in displaying in course of collision the ionizing density in both configuration and momentum spaces (see for instance [10]).

Nevertheless, the resulting quantum pictures remain less illustrative than the classical ones; a phase space trajectory with well-defined position $\mathbf{r}(t)$ and momentum $\mathbf{p}(t)$ cannot be associated to the motion of the ionized electron because of the indetermination inherent in

Heisenberg's quantum mechanics. In the present contribution, we circumvent this drawback by calculating the ionization current density $\mathbf{J}(\mathbf{r}, t)$ and define the average velocity field $\mathbf{v}(\mathbf{r}, t) = \mathbf{J}(\mathbf{r}, t)/\rho(\mathbf{r}, t)$ where $\rho(\mathbf{r}, t)$ is the ionizing density at point $\mathbf{r}$. This does not imply a continuous electronic trajectory throughout the collision but allows to establish at any time t the correspondence $\{\mathbf{r}, \mathbf{v}\}$ between electron position and average velocity. Illustrative arrow diagrams [7] $\{\mathbf{r}, \mathbf{v}\}$ can thus be displayed in course of collision and compared with their classical counterparts.

Comparisons of quantum and classical descriptions of density and current field are almost always analysed using the formal analogy of quantum and classical theories, stemming from the standard fluid dynamical interpretation of the Schrödinger equation [15,16]. Further the classical equations of motion are usually obtained from a limiting high momentum procedure on the quantal ones [15]. However, for the specific case of ionizing ion-atom collisions, we shall stress in the following section that the appropiateness of the CTMC description cannot lie on this limiting approximation since the electronic momentum is small. It is rather due to the statistical formulation of the problem, as employed e.g. in [17], that models the probabilistic quantum mechanical one and enables a fair reproduction of the physical dynamics by means of averaged density and current fields.

We address this point in section II of the present contribution. We outline in section III the CTMC method and the monocentric close-coupling spherical Bessel expansion, that yield very close descriptions of ionization, as illustrated in section IV for $He^{2+} + H(1s)$ collisions. Finally we show that both classical and quantal treatments asymptotically depict the ionization mechanism as a quasi free expansion of the cloud; further the phase of the quantum electronic wavefunction reproduces the 'exploding factor' $U = vr^2/2R$, as surmised in [8].

Atomic units are used throughout, unless otherwise stated.

II. CORRESPONDENCE OF CLASSICAL AND QUANTUM DESCRIPTIONS OF ELECTRONIC MOTION

As mentioned in the introduction, the usual connection between classical and quantum mechanics is obtained from the fluid dynamical interpretation of the Schrödinger equation [15,18]. We consider a single electron system and employ an eikonal treatment of the collision, in which the nuclear motion follows rectilinear trajectories and the electronic motion is described by the time-dependent Schrödinger equation:

$$i\frac{\partial\Psi(\mathbf{r},t)}{\partial t} = H\Psi(\mathbf{r},t) = \left(-\frac{1}{2}\nabla^2 + V\right)\Psi(\mathbf{r},t). \tag{1}$$

We write the wavefunction in its polar form:

$$\Psi(\mathbf{r},t) = \varrho_Q^{1/2}(\mathbf{r},t)\ \exp[iS_Q(\mathbf{r},t)], \tag{2}$$

yielding the well-known equations that are equivalent to eq.(1):

$$\frac{\partial S_Q}{\partial t} + \frac{(\nabla S_Q)^2}{2} + V = \frac{\nabla^2\varrho_Q^{1/2}}{2\varrho_Q^{1/2}} \tag{3}$$

$$\frac{\partial\varrho_Q}{\partial t} + \nabla\cdot(\varrho_Q\nabla S_Q) = 0 \tag{4}$$

where the second one is the continuity equation for the spatial density $\varrho_Q(\mathbf{r},t)$. We further define, in the usual way, the current density $\mathbf{J}_Q(\mathbf{r},t)$ and velocity field $\mathbf{v}_Q(\mathbf{r},t)$:

$$\mathbf{J}_Q(\mathbf{r},t) = \frac{i}{2}\left[\Psi^*(\mathbf{r},t)\nabla\Psi(\mathbf{r},t) - \Psi(\mathbf{r},t)\nabla\Psi^*(\mathbf{r},t)\right] = \nabla S_Q(\mathbf{r},t)\varrho_Q(\mathbf{r},t) = \mathbf{v}_Q(\mathbf{r},t)\ \varrho_Q(\mathbf{r},t). \tag{5}$$

We now consider the classical analogue. The standard procedure likens the probability distributions of the quantal formulation to those of a classical statistical mixture, which is obtained from a limiting high momentum procedure on the quantal equations, by neglecting the right-hand side of eq. (3):

$$\frac{\partial S_C}{\partial t} + \frac{(\nabla S_C)^2}{2} + V = 0 \tag{6}$$

One then obtains the Hamilton-Jacobi equation for the characteristic function $S_C(\mathbf{r},t)$. The Wentzel-Kramers-Brillouin (WKB, [15]) method of adding corrections to this function is also well known. However, in the present case this is not the most appropiate procedure, since, as reasoned in [19] the success of the classical approach does not lie in the high momentum limit of the quantal treatment (the momentum is small), but in the specific nature of the Coulomb interaction, which leads to additional symmetries and coincidences between quantum mechanical and classical statistical descriptions. The irrelevance of the classical limit may be seen by considering the initial state of the system $\Psi(\mathbf{r},t) = \psi(\mathbf{r})exp(-iEt)$ with ψ a stationary state of energy E. Then, eq. (1) becomes:

$$\nabla^2\psi = 2(V-E)\psi \tag{7}$$

and eq. (3) reads:

$$\frac{\partial S_Q}{\partial t} + \frac{(\nabla S_Q)^2}{2} + V = V - E \tag{8}$$

while from eq. (6) we obtain that the classical action is given by the line integral:

$$S_C(r,t) = \int \sqrt{2(E-V)}dr - Et \tag{9}$$

This classical result is in sharp disagreement with the quantal one, $S_Q = -Et, \nabla S_Q = \mathbf{0}$.

A better procedure is to follow the discrete trajectory representation [2,3] provided by a Gibbs ensemble of non-interacting particles, whose statistical distribution function $\varrho(\mathbf{r},\mathbf{p},t)$ fulfills the Liouville equation:

$$\frac{\partial\varrho(\mathbf{r},\mathbf{p},t)}{\partial t} = -[\varrho(\mathbf{r},\mathbf{p},t), H] \tag{10}$$

together with an appropiate initial condition. One can define spatial and momentum densities, and mean current and velocity fields by the procedure [20]:

$$\varrho_C(\mathbf{r},t) = \int \varrho(\mathbf{r},\mathbf{p},t)d\mathbf{p} \tag{11}$$

$$\varrho_C(\mathbf{p},t) = \int \varrho(\mathbf{r},\mathbf{p},t)d\mathbf{r} \tag{12}$$

$$\mathbf{J}_C(\mathbf{r},t) = \int \mathbf{p}\varrho(\mathbf{r},\mathbf{p},t)d\mathbf{p} = \mathbf{v}_C(\mathbf{r},t)\varrho_C(\mathbf{r},t) \tag{13}$$

Spatial density and current fulfill the continuity equation (4):

$$\frac{\partial\varrho_C}{\partial t} + \nabla\cdot\mathbf{J}_C = \frac{\partial\varrho_C}{\partial t} + \nabla\cdot(\rho_C\mathbf{v}_C) = 0 \tag{14}$$

but $\mathbf{J}_C(\mathbf{r},\mathrm{t}) \neq \varrho_C(\mathbf{r},t)\nabla S_C(\mathbf{r},t)$: the average velocity field $\mathbf{v}_C(\mathbf{r},t)$ is not a potential field anymore so that the Abrines-Percival classical formulation essentially differs from the standard one of textbooks [15].

This classical formulation is much more relevant than the standard one to ion-atom collisions. For instance, if we consider the initial H($1s$) state in $He^{2+} + H(1s)$ collisions, and since $\varrho_C(\mathbf{r},\mathbf{p},-\infty) = \varrho_C(\mathbf{r},p,-\infty)$, we have:

$$\mathbf{J}_C(\mathbf{r},-\infty) = \left[\int \widehat{\varrho}d\Omega_p\right]\left[\int p^3\varrho(\mathbf{r},p,-\infty)dp\right] = \mathbf{0} \tag{15}$$

in analogy with the quantal case. Furthermore, in the other limit $t\to\infty$, it was shown in [6,21] that ionization probabilities and momentum distributions are close to the quantum counterparts. Hence, we may infer that at intermediate times $\mathbf{J}_C \approx \mathbf{J}_Q$ and $\mathbf{v}_C \approx \mathbf{v}_Q$, and this will be confirmed in Section IV.

III. COLLISIONAL TREATMENTS

Our methods are based on the impact parameter approach, in which the projectile follows classical rectilinear trajectories with constant velocity $\mathbf{v}$ and impact parameter $\mathbf{b}$.

In the CTMC procedure, the electronic probability distribution is generated through a N-point discrete representation:

$$\varrho_C(\mathbf{r},\mathbf{p};v,b,t) = \frac{1}{N}\sum_{j=1}^{N}\delta(\mathbf{r}-\mathbf{r}_j(t))\delta(\mathbf{p}-\mathbf{p}_j(t)) \tag{16}$$

with an *hydrogenic* initial condition, for a target atom of nuclear charge Z_T:

$$\varrho_C(\mathbf{r},\mathbf{p};v,b,t\to-\infty) \;=\; \sum_{k=1}^{8}\; a_k\;\delta\left(E_k - \frac{p^2}{2} + \frac{Z_T}{r}\right) \tag{17}$$

where the energies E_k and coefficients a_k are chosen so as to achieve good approximations to the spatial and momentum quantum densities [22,23]. In practice, we used $N = 40000$ independent electronic trajectories to generate the probability distribution.

Substitution of (16) in the Liouville equation (10) for the collision Hamiltonian $H = H_0 + V_P$, with $H_0 = -\nabla^2/2 - Z_T/r$ the target Hamiltonian and $V_P = -Z_P/|\mathbf{r}-\mathbf{b}-\mathbf{v}t|$ the electron-projectile interaction, yields the well-known Hamilton equations for the N independent trajectories $\{\mathbf{r}_j(t), \mathbf{p}_j(t)\}$. The ionizing part $\varrho_C^{ion}(\mathbf{r}, \mathbf{p}; v, b, Z)$ of the classical distribution is obtained as a function of the scaled time $Z = vt$ under the time-dependent energy conditions $E_T = p^2 - Z_T/r > 0$, $E_P = (\mathbf{p}-\mathbf{v})^2 - V_P > 0$. Spatial, momentum and mean current densities are then obtained by performing the integrations of eq. (11), (12), (13) and a local averaging procedure over $\mathbf{r}$ or $\mathbf{p}$ to obtain statistically convergent results. This averaging employs small cubes about $\mathbf{r}$ and $\mathbf{p}$, respectively, and therefore only involves a small number of particles. In previous work [7,8], we employed arrow diagrams $\mathbf{p}_j(\mathbf{r}_j)$ to illustrate the collisional mechanisms. At sufficiently large internuclear distances such that the statistical particles are well separated, there is only one electron in each cell, so that the momentum $\mathbf{p}_j(\mathbf{r}_j)$ and (averaged) velocity $\mathbf{v}_C(\mathbf{r})$ representations are equivalent.

Our semi-classical treatment consists of a monocentric close-coupling scheme that provides a very accurate representation of the atomic spectrum and recently led to a reliable description of the electronic flux throughout $\bar{p}+H(1s)$ collisions [10]. The total wave function is expanded in terms of target eigenstates $\psi_{E_nlm}(\mathbf{r})$:

$$\Psi(\mathbf{r}, v, b, t) = \sum_{E_nlm} a_{E_nlm}(v, b, t)\psi_{E_nlm}(\mathbf{r})e^{-iE_nt} \tag{18}$$

with $E_n =< \psi_{E_nlm}|H_0|\psi_{E_nlm} >$. The atomic eigenstates are obtained by diagonalization of H_0 in a basis of spherical Bessel functions confined in a spherical box of radius $r_{max} = 120$ a.u. centred on the target. In practice, the underlying basis consists in all the $j_l(kr)$ functions such that $j_l(kr_{max}) = 0$ with $0 \le k \le k_{max} = 2.5$ a.u. and $0 \le l \le l_{max} = 5$. Spherical harmonics are included up to $m_{max} = 2$, yielding 1420 states, and $1s$ and $2p$ bound eigenstates have been added to this basis before diagonalizing H_0 to speed up the convergence of the expansion with respect to the description of the lowest bound eigenstates. The convergence of all the following results with respect to the parameters $\{r_{max}, k_{max}, l_{max}\}$ of the underlying basis has been explicitely checked as in [10].

The ionizing part $\Psi^{ion}(\mathbf{r}, v, b, t)$ of the total wave function is obtained from (18) under the restriction $E_n > 0$. For positively charged ion impact, such a condition does not provide a separation of the capture and ionization fluxes and $\Psi^{ion}(\mathbf{r}, v, b, t)$ accounts for the total electron loss from the target; accordingly, we focus hereinafter on high energy $He^{2+} + H(1s)$ collisions where the charge exchange process is negligible compared to the ionization one. Furthermore, we explicitely checked using CTMC calculations that the omission of the remaining condition $E_P > 0$ does not distort any of our illustrations. The wave function in momentum space $\Psi^{ion}(\mathbf{p}, v, b, t)$ is computed by (Fast) Fourier Transform of Ψ^{ion}. The ionizing density is trivially obtained as $\varrho_Q^{ion} = |\Psi_Q^{ion}|^2$ in both configuration and momentum spaces, and the current density $\mathbf{J}_Q(\mathbf{r}, t)$ and velocity field $\mathbf{v}_Q(\mathbf{r}, t)$ are calculated according to eq. (5).

IV. RESULTS AND DISCUSSION

Our illustrations are drawn for $He^{2+} + H(1s)$ collisions and an impact velocity $v = 3$ a.u.. For this velocity, the total ionization cross sections obtained by means of the CTMC and monocentric Bessel calculations are 2.748 10^{-16} and 2.750 10^{-16} cm^2 respectively. We further display in Fig. 1a the corresponding weighted probabilities $bP^{ion}(b)$ as functions of the impact parameter b. Quantum and classical results compare favourably even though some well-known discrepancies appear, that are inherent in the classical description of ionization in fast ion-atom collisions, such as the lack of long range dipolar ionizing transitions and the overestimation of the probability at small b [24]. Both the CMTC and monocentric Bessel calculations exhibit a maximum contribution to the cross section around $b = 1.5$ a.u.; the rectilinear trajectory defined by ($v = 3$ a.u., $b = 2$ a.u.) will be therefore considered as representative in the following illustrations of the ionization dynamics at $v = 3$ a.u..

We present in Fig. 1b the temporal evolution of the classical and quantum ionization probabilities along this nuclear trajectory. Both descriptions agree in predicting that all ionizing events occur quite suddenly as the projectile crosses the target domain from $Z = -5$ a.u. to $Z = 10$ a.u.. We are thus led to conclude in favour of the universality of this feature which already appeared in low velocity $He^{2+} + H(1s)$ collisions [8] as well as in $\bar{p} + H(1s)$ collisions [10].

We report in Fig. 2 some snapshots of the ionizing density in the quantum and classical calculations. Electron distributions are displayed in both configuration and momentum spaces to get further insights on the ionization dynamics. Moreover, we make use of reflection symmetry with respect to the (x, z) collisional plane, with $\hat{\mathbf{x}} = \hat{\mathbf{b}}$ and $\hat{\mathbf{z}} = \hat{\mathbf{v}}$, and present two-dimensional distributions, $\varrho^{ion}(x, z)$ and $\varrho^{ion}(p_x, p_z)$, obtained by integrating the 3D densities over the perpendicular coordinates y and p_y respectively.

It is clear from the figures that the present CTMC and monocentric Bessel calculations yield similar ejected electron distributions throughout the collision and depict the same ionization mechanism: a part of the electron cloud, polarized by the incoming projectile across the turning point, picks up enough energy to detach from the target but does not succeed in following adiabatically the swift projectile; it is thus left behind in an ionized state. The ionizing cloud then starts to rotate around the target, pulled ahead by the outgoing projectile and subject to the fixed-target nucleus field. The equations of motion had to be integrated up to large internuclear distances ($Z = 150$ a.u.) to reach the asymptotic region where the momentum distributions no longer change significantly. This emphasizes the long range influence of Coulomb forces on the asymptotic distribution, oftenly referred to as post collision interaction (PCI) effects, while the probability reaches its asymptotic value much earlier. PCIs induce further changes in the quantum distributions, as illustrated in Fig. 2 from $Z = 50$ to 150 a.u., so that the classical cloud tends to its final conformation faster than the quantum one. In fact, the quantum momentum distribution lags slightly behind its classical couterpart since the early stages of the ionization process (see $Z = 0$ a.u. in Fig. 2). We thus display in Fig. 3 the classical and quantum distributions at the very beginning of the mechanism, *i.e.* at time $Z = -2$ a.u.. In the classical framework, binary electron-projectile interactions are of paramount importance and the ionizing electrons are those which lie in the near neighbourhood of the projectile. They are mainly emitted in the positive transverse direction while passing round the projectile. The configuration and momentum classical distributions do not show a proper polarization drift towards the projectile starting from an isotropic initial cloud with $\mathbf{J}_C(\mathbf{r}) = 0$, while the quantum ones exhibit similar shapes in configuration and momentum spaces, along the internuclear axis. In the quantum framework ionization arises as a result of a strong polarization of the cloud towards the projectile, and involves a combined outflow of the whole cloud. From that time onwards the evolution of the ionizing density is determined by the combined field of the nuclei and similarly reproduced by the classical and quantum treatments. The trace of the initial advance of the classical distribution with respect to the classical one is still visible in course of collision but finally dies off in the asymptotic region where the ionizing density stabilizes close to the target, in the left upper quadrant of both configuration and momentum spaces.

We now go deeper into our comparison of quantum and classical dynamics and display in Fig. 4 a time sampling of the velocity fields $\mathbf{v}_Q(\mathbf{r}, t)$ and $\mathbf{v}_C(\mathbf{r}, t)$. We restrict our illustration to the ionizing electrons that lie in the $y = 0$ collision plane, approximated to a thin slab $-\varepsilon \leq y \leq \varepsilon$ within the classical (statistical) calculations. Furthermore the velocity fields are only drawn in the space regions where $\varrho^{ion}(x, z, t) \geq \varrho^{ion}_{max}/10$, with ϱ^{ion}_{max} the maximum of the ionizing density in the $y = 0$ plane.

The first velocity diagrams of Fig. 4 clearly exhibit how ionization arises, from a drift of the cloud towards the projectile. The most strinking feature of the quantum velocity field is its laminar nature in the vinicity of the projectile which does not act like a scattering center (the center concept is reviewed in [1]). Reversely and as previously stated, the classical approximation overstates the scattering influence of the projectile about which electrons are locally scattered and ionized. Nevertheless this small discrepancy does not have critical repercussions on the subsequent behaviour of the ionizing cloud: as soon as electrons are ionized, they are pulled ahead by the outgoing projectile; on the left side of the longitudinal wake induced by the pulling projectile, inner electrons ($x < b$) are strongly subject to the target field and experience a strong deflection by this center while on the other side, outer electrons ($x > b$) escape in the $p_x > 0, p_z > 0$ direction (see the $Z = 10$ a.u. snapshots in Fig. 4). The salient feature of the following velocity diagrams of Fig. 4 is an isotropic expansion of the cloud, in which position $\mathbf{r}$ and velocity $\mathbf{v_{Q,C}}$ vectors point at the same direction, except in the target zone where ionizing trajectories are still being deflected. Finally both quantum and classical treatments describe the ionization mechanism as a quasi uniform expansion from the inner target-centered region, so that $\mathbf{r} \sim \mathbf{v}_{Q,C}t$. In analogy to the "big bang" description of universe expansion [8], the quasi free expansion picture of the ionization mechanism can be strenghtened by the fact that, viewed from any origin, all electrons appear to be rushing away from it. We illustrate this point in Fig.5 which reports the last diagrams of Fig.4 with the origins of momenta at the target (T), center of nuclear force (SP) and projectile (P) values, respectively.

It was pointed out in [8,25] and elicited in [10,26] that finite close-coupling expansions in terms of exponentially decaying basis functions do not provide an accurate description of the ionization process because of their inability to reproduce the expansion of the ionizing cloud at large Z. Electron translation factors [27,28] are oftenly introduced in such expansions to account for the average motion of the electron cloud. It was reasoned in [8] that neither the usual Common Translation Factors (CTF, [28,29]) nor the Plane Wave Translation one (PWTF, [27]) are suitable to represent the ionizing mean velocity field in the asymptotic region, and a simple phase factor $S^{exp}(\mathbf{r}, t) = vr^2/2R$, fulfilling $\nabla S^{exp} \longrightarrow \mathbf{r}/t$ as $t \longrightarrow \infty$, and describing a free expansion, was proposed. In fact, this factor was already included in the formulation of the advanced adiabatic approximation [30] to fulfill the correct boundary conditions. It leads to an invariance of the wavefunction with respect to Fourier transform [31], which appears in the classical formalism through the time scaling $\mathbf{r} = \mathbf{p}t$ of the configuration and momentum distributions. We now show that the same factor is obtained from our ionizing wavefunction; in this respect, it should be noted that the expansion (18) contains no translation factors. For this purpose, we consider the phase $S_Q(\mathbf{r}, t)$ of the wavefunction (see eq. (2)), and draw in Fig. 6 for $Z = 150$ a.u. the spherical components of $\nabla S_Q(\mathbf{r}, t)$, as functions of the scaled variable r/R, along specific directions (θ_i, ϕ_i) with $\theta_i \in [0, \frac{\pi}{4}, \frac{\pi}{2}, ..., \pi]$ and $\phi_i \in [0, \frac{\pi}{4}, \frac{\pi}{2}, ..., 2\pi]$. The average behaviour of the three components can be accurately fitted by the predictions for the free expansion factor: $\mathbf{u}_r \nabla S^{exp} = vr/R$, $\mathbf{u}_\theta \nabla S^{exp} = 0$ and $\mathbf{u}_\phi \nabla S^{exp} = 0$. Moreover, we note that the corresponding expressions $\mathbf{u}_r \nabla S^{PWTF} = pvcos\theta$, $\mathbf{u}_\theta \nabla S^{PWTF} = -pvsin\theta$ for a plane-wave translation factor are totally inadequate. The present quantum calculations, free of any ETFs, thus reinforce the adequation of the common phase factor $S^{exp}(\mathbf{r}, t) = vr^2/2R$ to the representation of the ionizing asymptotic velocity field. Large deviations from free expansion are obviously found for $r/R \leq 0.1$ where the electrons are strongly subject to the target field. Far away from this center ($r/R \sim 0.45$), the ionizing density is extremely low (see Fig. 2) and correspond to fast electrons which fair representation would require the use of a largest Bessel set ($k_{max}, l_{max} \longrightarrow \infty$); despite spurious oscillating structures in Fig. 6, we did not try to improve the representation of these electrons that do not contribute significantly to the global ionization process.

V. CONCLUSIONS

Scenarios of electron production in ionizing $He^{2+} + H(1s)$ collisions at the threshold of the high impact energy range have been obtained by implementing state-of-the-art CMTC and close-coupling methods. They have been first illustrated by means of time samplings of the spatial and momentum ionizing densities. We further calculated the ionization current density $\mathbf{J}(\mathbf{r}, t)$ and corresponding velocity field $\mathbf{v}(\mathbf{r}, t)$ and snapshotted the ionizing cloud in course of collision. Intuitive arrow diagrams $\{\mathbf{r}, \mathbf{v}\}$ have thus been displayed to reveal distinctly the electron dynamics.

We emphasized that the classical and quantum mechanical treatments of electronic motion yield very close descriptions of both the ionizing density and velocity field. Electrons are emitted as they fail to be captured when the nuclei are closest; after this the main feature of the mechanism is a quasi free expansion of the cloud, even though weak but long-range postcollision interactions induce a rotation of the cloud about the target. In the asymptotic region, the velocity field thus fulfills $\mathbf{v}(\mathbf{r},t) \sim \mathbf{r}/t$ and the common phase of the quantum wavefunction reproduces the free expansion factor $vr^2/2R$.

As we traced back to the origin of the ionizing events, we found that CTMC calculations overstate the scattering influence of the projectile. Under the present impact conditions, this does not have serious consequences on the subsequent evolution of the ionizing cloud. We plan to check whether this feature holds for higher impact velocities and other impinging ions, with the aim to mark out distinctly the validity range of the classical approximation. The use of the same tools as in the present work would nicely complement previous studies that mostly focused on asymptotic features of differential cross sections (see e.g. [24] and references therein).

ACKNOWLEDGMENTS

One of us (C.I.) would like to acknowledge the Ministerio de Educación y Cultura, Spain, for a Postdoctoral grant under the program SEEUID.

REFERENCES

[1] N. Stoltherfoht, R. D. DuBois and R. D. Rivarola, *Electron Emission in Heavy Ion-Atom collisions*, Springer, Berlin (1997)

[2] R. Abrines and I. C. Percival, Proc. Phys. Soc. London **88**, 861 (1966)

[3] R. E. Olson and A. Salop, Phys. Rev. A **16** 531 (1977)

[4] G. W. Kerby III, M. W. Gealy, Y.-Y. Hsu, M. E. Rudd, D. R. Schultz and C. O. Reinhold, Phys. Rev. A **51** 2256 (1995)

[5] S. D. Kravis, M. Abdalallah, C. L. Cocke, C. D. Lin, M. Stockli, B. Walch, Y. D. Wang, R. E. Olson, V. D. Rodriguez, W. Wu, M. Pieksma and N. Watanabe, Phys. Rev. A **54** 1395 (1994)

[6] C. Illescas and A. Riera, Phys. Rev. A **60** 4546 (1999)

[7] C. Illescas, I. Rabadán, and A. Riera, J. Phys. B **30** 1765 (1997); Phys. Rev. A **57**, 1809 (1998)

[8] C. Illescas and A. Riera, Phys. Rev. Lett. **80**, 3029 (1998); erratum **81** 1350 (1998);

[9] G. Bandarage and R. Parson, Phys. Rev. A **41** 5878 (1990)

[10] B. Pons, Phys. Rev. Lett. **84**, 4569 (2000); Phys. Rev. A **63**, 012704 (2001)

[11] G. Schiwietz, Phys. Rev. A **42** 296 (1990)

[12] O. J. Kroneisen, H. J. Ludde, T. Kirchner and R. M. Dreizler, J. Phys. A **32** 2141 (1999)

[13] J. C. Wells, D. R. Schultz, P. Gavras and M. S. Pindzola, Phys. Rev. A **54**, 593 (1996)

[14] E. Y. Sidky and C. D. Lin, J. Phys. B **31**, 2949 (1998)

[15] A. Messiah, *Mécanique Quantique*, Dunod, Paris (1959)

[16] H. Goldstein, *Classical Mechanics*, Addison-Wesley Publishing Company (1950)

[17] S. Brandt and H. D. Dahman, *The picture book of Quantum Mechanics*, Springer-Verlag, New-York (1995)

[18] C. O. Reinhold and C. A Falcón, J. Phys. B **21** 1829 (1998)

[19] B. H. Bransden and M. H. C. McDowell, *Charge Exchange and the Theory of Ion-Atom Collisions*, Oxford Science Publications, Oxford (1992)

[20] P. M. Morse and H. Feshbach, *Methods of Theoretical Physics*, McGraw-Hill (1953)

[21] E. Y. Sidky, C. Illescas and C. D. Lin, Phys. Rev. Lett. **85**, 1634 (2000)

[22] D. J. W. Hardie and R. E. Olson, J. Phys. B **16**, 1983 (1983)

[23] G. Duchateau, C. Illescas, B. Pons, E. Cormier and R. Gayet, J. Phys. B **33**, L571 (2000)

[24] C. O. Reinhold and J. Burgdorfer, J. Phys. B **26** 3101 (1993)

[25] A. Riera, Comments on Atomic and Molecular Physics **1** 131 (2000)

[26] E. Y. Sidky and B. D. Esry, Phys. Rev. Lett. **85** 5086 (2000)

[27] D. R. Bates and R. McCarroll, Proc. R. Soc. A **245** 175 (1958)

[28] S. B. Schneidermann and A. Russek, Phys. Rev. **181** 311 (1969)

[29] L. F. Errea, C. Harel, H. Jouin, L. Méndez, B. Pons and A. Riera, J. Phys. B **27** 3603 (1994)

[30] E. A. Solov'ev, in *The Physics of Electronic and Atomic Collisions, XIX International Conference*, edited by L. J. Dubé, J. B. A. Mitchell, J. W. McConkey and C. E. Brion, Whistler, Canada (1995)

[31] T. P. Grozdanov and E. A. Solov'ev, Eur. Phys. J. D **6** 13 (1999)

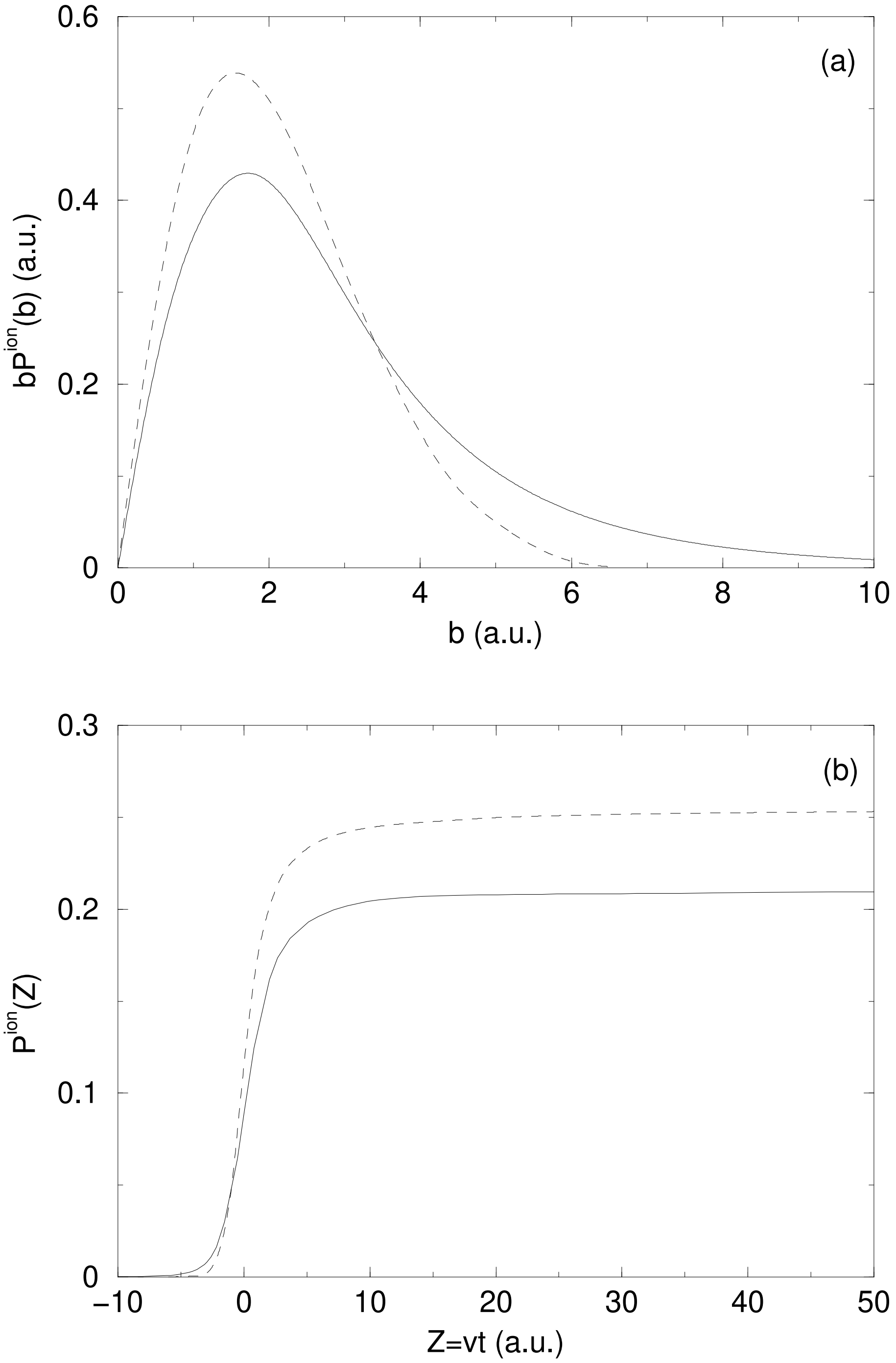

Figure 1: (a) Weighted probability $bP^{ion}(b)$ for ionization in $He^{2+} + H(1s)$ collisions for an impact velocity $v = 3$ a.u., as a function of the impact parameter b and (b) Temporal evolution of the ionization probability $P^{ion}(Z)$ along the rectilinear nuclear trajectory ($v = 3$ a.u., $b = 2$ a.u.), as a function of the scaled time $Z = vt$: (——) quantum and (– – –) CTMC calculations.

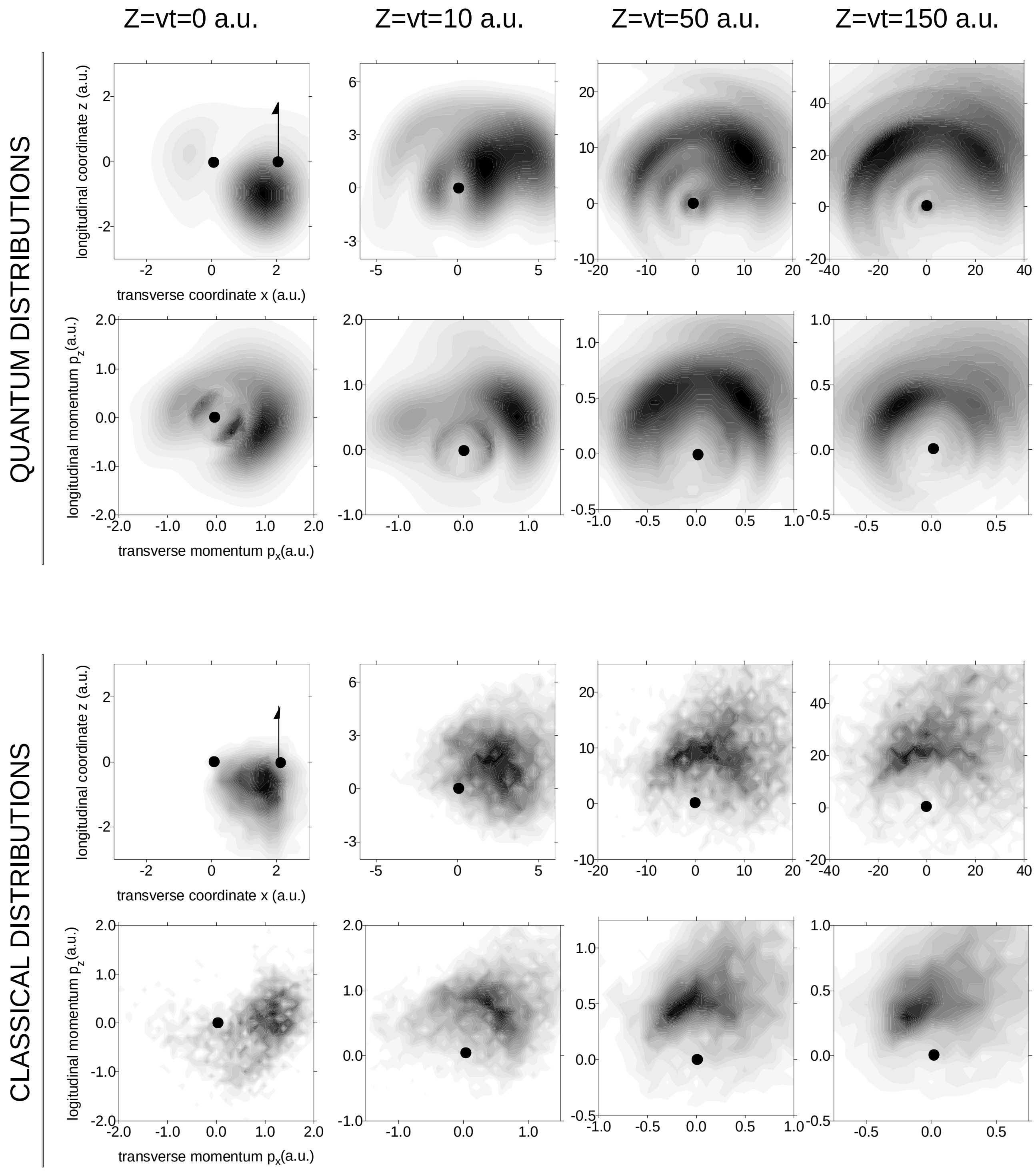

Figure 2: Quantum (top) and classical (bottom) two-dimensional distributions of ejected electrons in configuration and momentum spaces, as a function of the scaled time $Z = vt$, for $He^{2+} + H(1s)$ collisions, $v = 3$ a.u. and $b = 2$ a.u.. The black points indicate the nuclear positions.

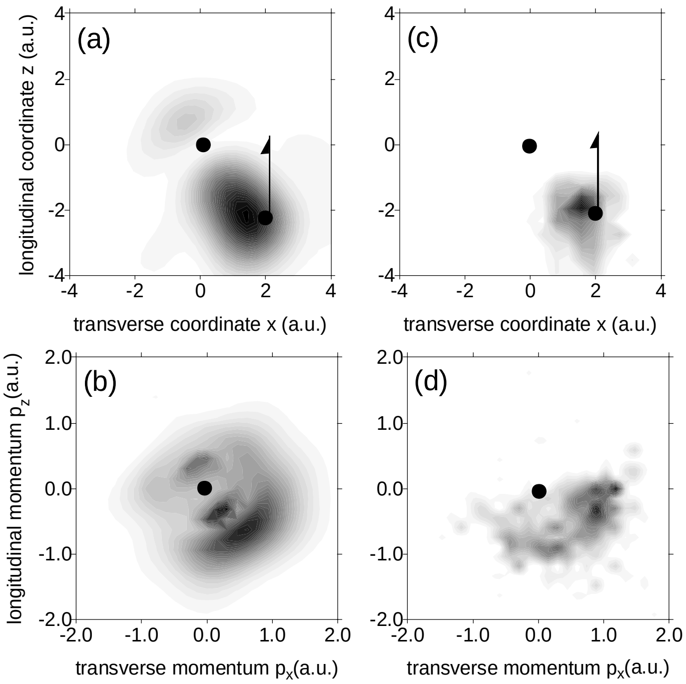

Figure 3: Quamtum (a-b) and classical (c-d) two-dimensional distributions of ejected electrons in configuration and momentum spaces, for $He^{2+} + H(1s)$ collisions, $v = 3$ a.u., $b = 2$ a.u. and $Z = -2$ a.u.. Nuclear positions are indicated ($\bullet$).

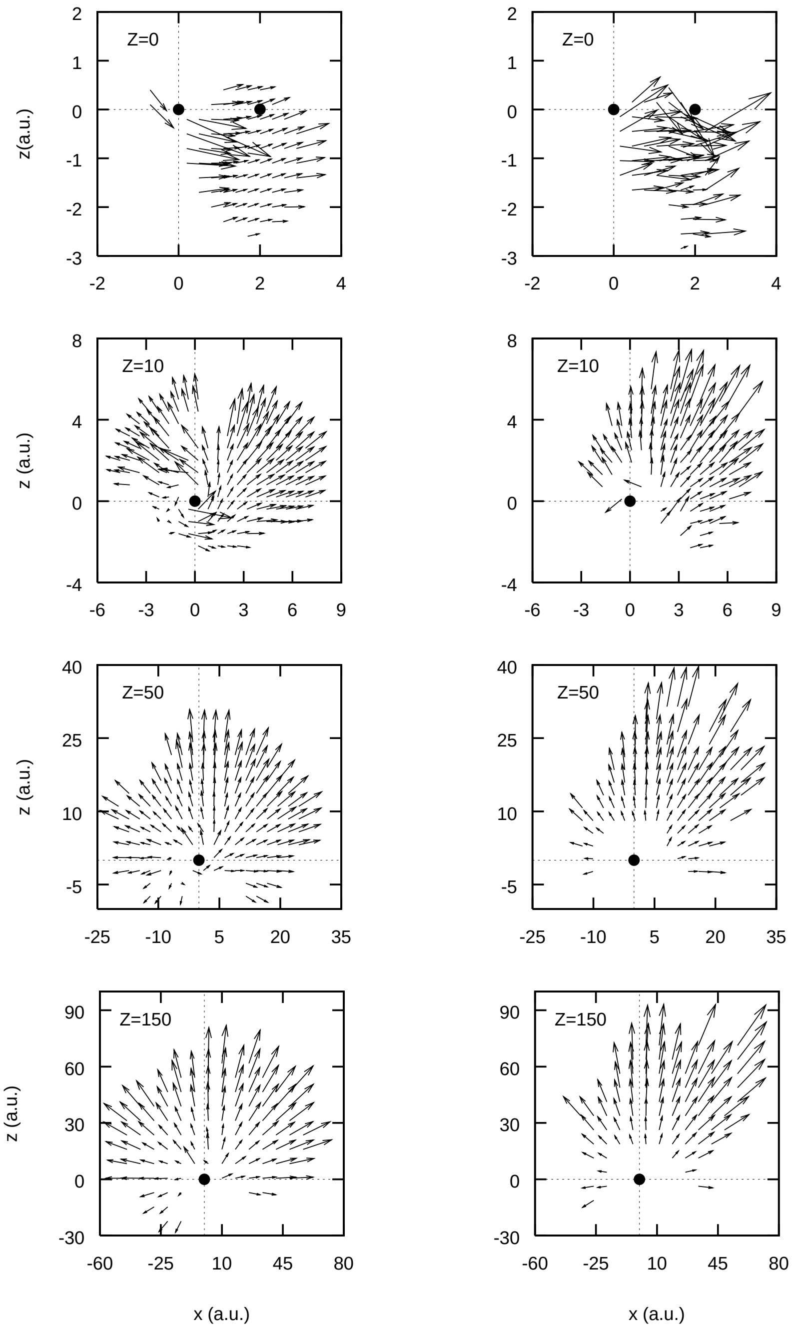

Figure 4: Quantum (left) and classical (right) velocity diagrams $\{\mathbf{r}, \mathbf{v}_{Q,C}\}$ for the ionizing electrons that lie about the collision plane in $He^{2+} + H(1s)$ collisions, along the nuclear trajectory (v = 3 a.u., b = 2 a.u.). The velocity vectors are multiplied by the a scaling factor ℓ= 0.8, 1, 3 and 15 au for $Z = 0,\ 10,\ 50$ and 150 a.u. respectively. The momenta are defined with respect to the target which is at rest and nuclear positions are indicated ($\bullet$).

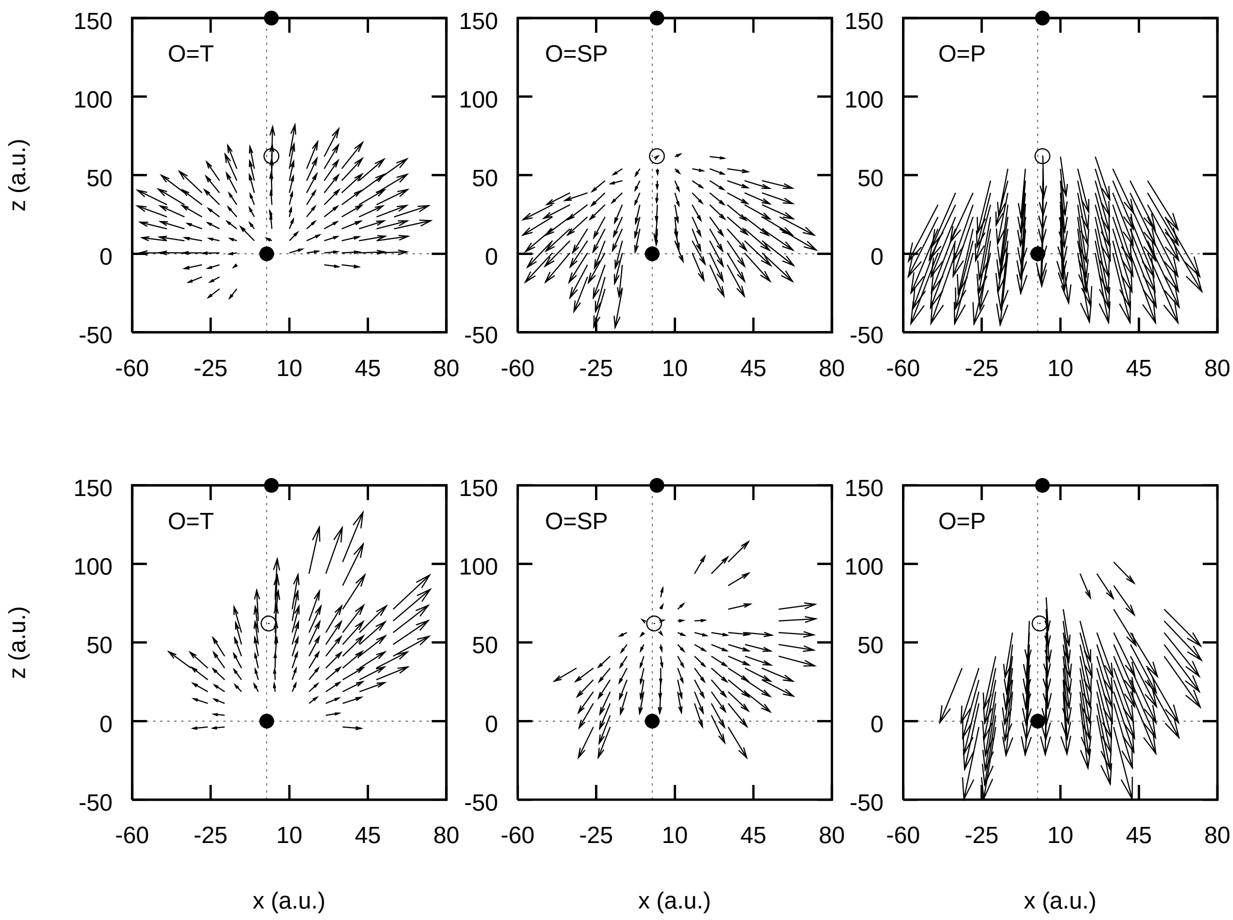

Figure 5: Quantum (top) and classical (bottom) velocity diagrams for the ionizing electrons that lie about the collision plane in $He^{2+} + H(1s)$ collisions, $v = 3$ a.u., $b = 2$ a.u. and $Z = 150$ a.u.. The momenta are simultaneously defined with respect to the target (O=T, $\bullet$), to the center of force (O=SP, $\bigcirc$) and to the projectile (O=P, $\bullet$).

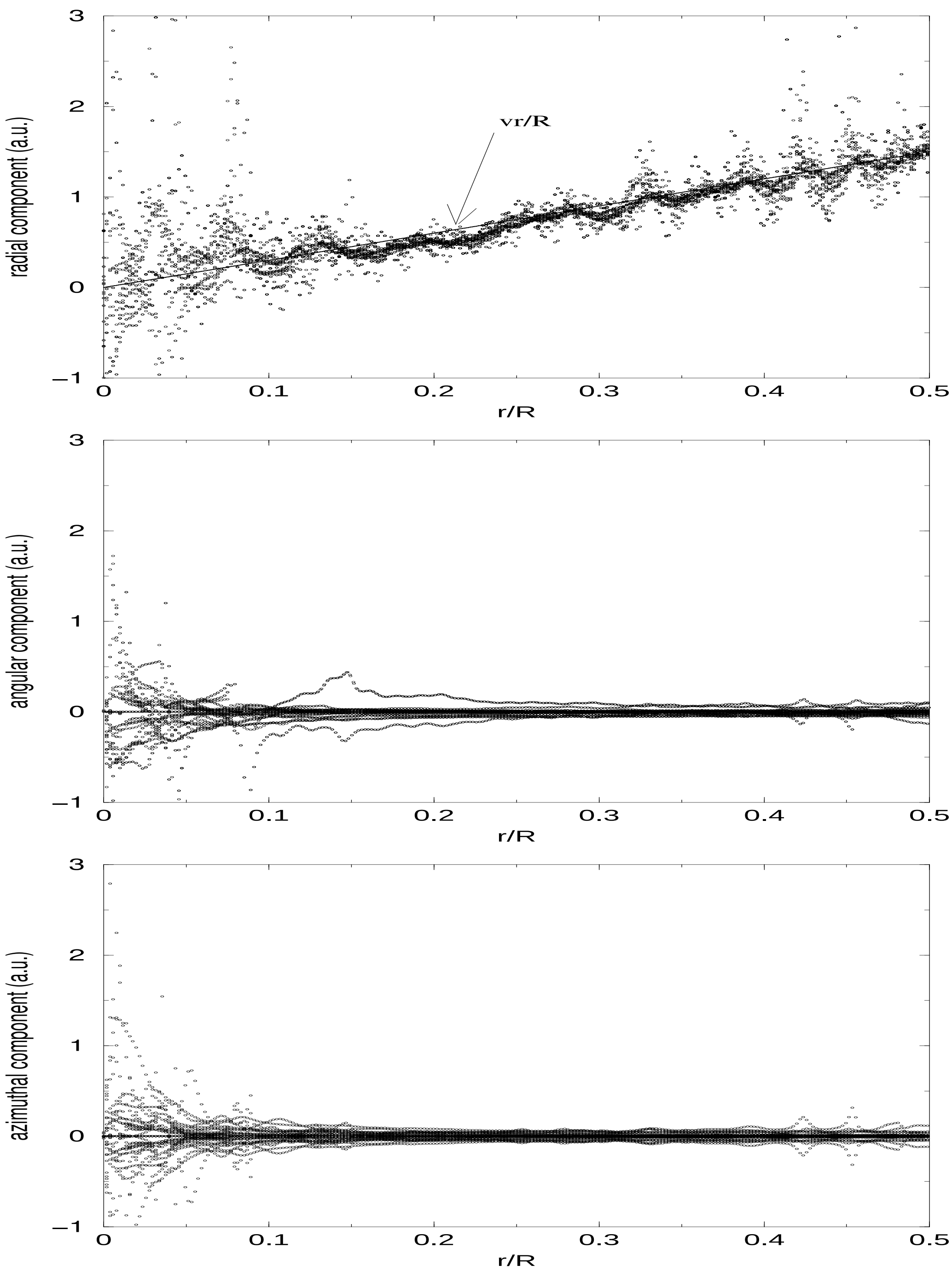

Figure 6: Spherical components of $\nabla S_Q(\mathbf{r},t)$ with $S_Q(\mathbf{r},t)$ the common phase of the ionizing quantum wave function for $He^{2+} + H(1s)$ collisions, $v = 3$ a.u., $b = 2$ a.u. and $Z = 150$ a.u., as functions of the scaled variable r/R and along specific directions (θ_i, ϕ_i) with $\theta_i \; \epsilon \; [0, \frac{\pi}{4}, \frac{\pi}{2}, ..., \pi]$ and $\phi_i \; \epsilon \; [0, \frac{\pi}{4}, \frac{\pi}{2}, ..., 2\pi]$.